Task T4.1 - Deliverable D4.1

Report on the predicting capabilities of the standard simulation tools in the 150-600 MeV energy range

J.-C. David[1], A. Boudard[1], J. Cugnon[2], S. Leray[1], D. Mancusi[2]

[1] CEA/Saclay, IRFU/SPhN, 91191 Gif-sur-Yvette Cedex, France

[2] University of Liège, AGO Department, allée du 6 Août 17, bât. B5, B-4000 Liège 1, Belgium

Abstract: During the NUDATRA project, new versions of the INCL4 intranuclear cascade and ABLA de-excitation models were developed in view of improving the prediction capabilities of the simulation codes used for the design of ADS spallation targets. The quality of the models has been confirmed by a recent benchmark organized by IAEA. However, most of the effort has been devoted to improving the models around 1 GeV paying less attention to the 150-600 MeV region which appears important for the design of the MYRRHA ADS demonstrator. In this report, we review the existing experimental data in the 150-600 MeV energy region and compare them to the predictions of INCL4-ABLA07. This allows establishing some specific remaining deficiencies, which will be addressed in Task 4.4.

1. Introduction

Large efforts have been devoted during the FP5-HINDAS [Meu05] and FP6-EUROTRANS/NUDATRA [NUD04] projects to collecting high quality data and improving the physics of spallation models in view of providing reliable simulation tools for ADS design. At the end of NUDATRA, new versions of the INCL4 intranuclear cascade and ABLA de-excitation models, INCL4.5 [Cug09] and ABLA07 [Kel09], are available which represent a significant progress compared to the previous versions. These models have been implemented into a private version of MCNPX [Hen05]. The most noticeable improvements concern the prediction of light charged particles (LCPs) and intermediate mass fragments (IMFs) [Cug10]. As regard LCPs, both the production rates and the energy spectra, including the high-energy tail, of the hydrogen and helium isotopes are now correctly predicted [Ler10a]. The production cross-sections of intermediate mass fragments were severely underestimated by the previous models, sometimes by several orders of magnitude, and are now much better predicted, although still not yet totally satisfactorily. A comprehensive comparison of the INCL4.5-ABLA07 combination to a wide set of experimental data covering different mass and energy regions, and different exit channels, a lot of them measured within the former FP5-HINDAS and NUDATRA projects, has been done in the framework of the benchmark of spallation models recently organized under the auspices of the International Atomic Energy Agency (IAEA) [IAE09]. The objective of this benchmark was to assess the prediction capabilities of the different spallation models used (or which could be used) in high-energy transport codes. The results have shown [Dav10a, Ler10b] that INCL4.5-ABLA07 was one of the best codes in particular for the prediction of residues, even if it was also stressed that there is still room for improvement.

However, most of the work done during these projects was focused on reactions around 1 GeV, mainly because this was the energy foreseen for the final ADS transmuter. Less has been done concerning the 150-600 MeV energy domain, which, actually, is of interest for demonstrator facilities and in particular the MYRRHA facility [DeB11] to be built in Mol, Belgium. In the MYRRHA project, a 4-5 mA 600 MeV proton beam will be sent into a liquid Pb-Bi spallation target.

In the ANDES project, WP4 is devoted to the improvement and validation of the INCL4-ABLA model in the 150-600 MeV energy domain, evaluated data library being supposedly used below 150 MeV. The first task is obviously to establish the state-of-the-art regarding the prediction capabilities of the nuclear models used in standard transport codes in this domain. This is the subject of the present report, in which some of the results from the IAEA Spallation Model Benchmark have been used, complemented by specific comparisons of the INCL4.5-ABLA07 models to available additional elementary data (part of them measured during the HINDAS and NUDATRA projects) in the 150-600 MeV energy domain. The goal is to identify remaining deficiencies that should be tackled during the ANDES project in order to further improve the predicting capabilities of the simulation tools for MYRRHA design, with emphasis on key parameters of the spallation target. These key parameters include: the spallation neutron yield; the total activity and major contributors to the activity of the target and structure materials; the production rate of helium (mostly for material damage assessment) and of radioactive gases, in particular tritium and volatile elements from the liquid target.

2. Neutron production

2.1 Lessons from the IAEA benchmark

In the IAEA benchmark, there was only one set of neutron production data proposed for comparison to models in the 150-600 MeV energy range, actually at 256 MeV. The data and results from the models having participated to the benchmark are displayed in Fig.1 and show an overall good agreement.
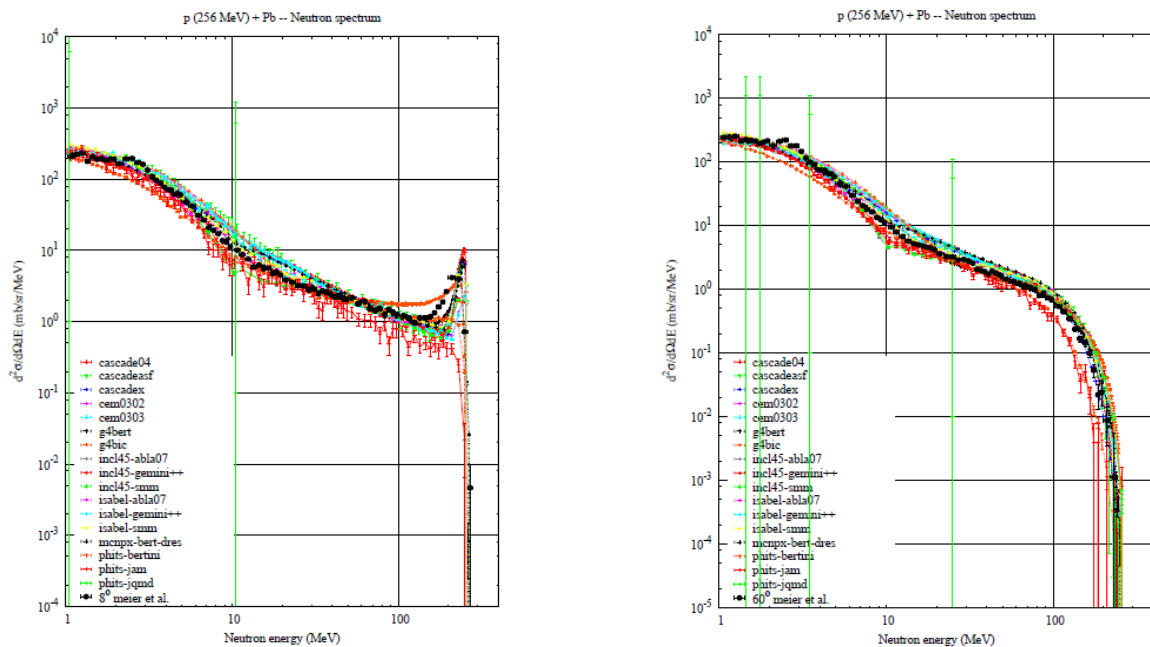

Figure 1: *Neutron double-differential cross-section at 8° (left) and 60° (right) for p (256 MeV) + Pb from [Mei93] compared to all the models which participated to the IAEA benchmark [IAE09].*

More generally, it was shown that neutron production double-differential cross-sections are rather well predicted, within 15 to 30% for most of the models, in both shape and level at all incident

energies. The agreement becomes better and better with increasing incident energy, some significant deviations appearing below 100 MeV and for specific regions of the energy spectrum such as the quasi-elastic and quasi-inelastic peaks at forward angles. As regards evaluation of the different models, a global coarse eye-guided rating was made, dividing each set of data into four energy bins representative respectively of the evaporation, pre-equilibrium, pure cascade and quasi-elastic regions [Dav10a, Ler10b]. Quality points were given: 2 for good, 1 for moderately good, minor problems, -1 for moderately bad, particular problems, and, -2 for unacceptably bad, systematically wrong. An average rate was obtained by dividing by the total number of bins. The result is presented in Fig.2 and shows that INCL4.5-ABLA07 is one of the best models.
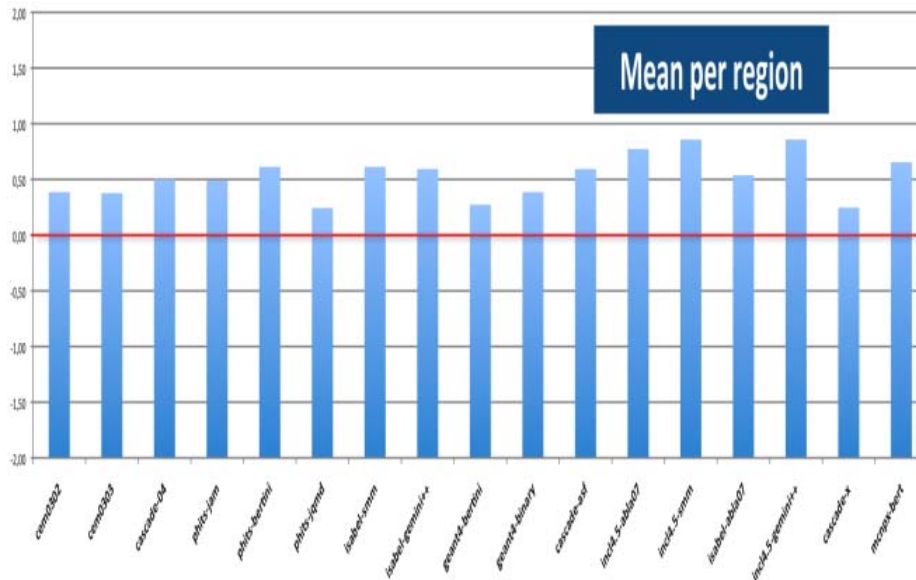

Figure 2: *Rating results obtained from the global coarse eye-guided analysis of the IAEA benchmark results [Dav10a, Ler10b] for neutron DDXS.*

2.2 Comparison to additional data sets

Unfortunately, there are not many data sets available in the energy range of present interest. In Fig. we compare our model to experimental data obtained at 597 MeV on both Fe and Pb [Ami93]. It can be seen, as expected from the conclusions of the benchmark, that INCL4.5-ABLA07 gives a very good agreement with the data at all angles. In order to better see the low energy part of the spectrum, which represents the major part of the emitted neutrons, an expanded view is presented in the right panel for the Pb target. It shows a slight underprediction of the model between 10 and 30 MeV.

Apart from data at 256 MeV on other targets than lead, there exists data at 160 MeV on Al, Zr and Pb [Sco90] and neutron-induced DDXS at 150 MeV on Fe from [Ara07]. The data on iron at 256 MeV are plotted in the left panel of Fig. 4 with an extended view of the low energy part of the spectrum in the middle panel. Our model agrees very well with the data in the evaporation region and at large angles. At forward angles, the agreement is much less good: the quasi-elastic peak is clearly too sharp and extends towards too large angles; a noticeable underprediction is visible in the intermediate energy region.

In Fig.4 right, data on neutron production induced by 150 MeV neutrons are presented. It should be noticed that in the experimental data the evaporation component is not isotropic, which could indicate a problem of normalization in the experiment, probably at the smallest angles. We can however at least compare the shape of the calculated spectra to the experimental ones and it can be observed that the agreement is not as good as at 256 MeV, prefiguring what was observed at lower energies in the benchmark. In particular, a discontinuity is found in the neutron spectra around 10

3

MeV, which, actually, is worsening when going to lower incident energies producing a clear spurious hole below 100 MeV incident energy. It is in fact due to a condition in INCL that forbids nucleons to undergo further collisions if they fall below a certain energy threshold. However, simply removing this condition has some (bad) effect on residue production at high incident energies.
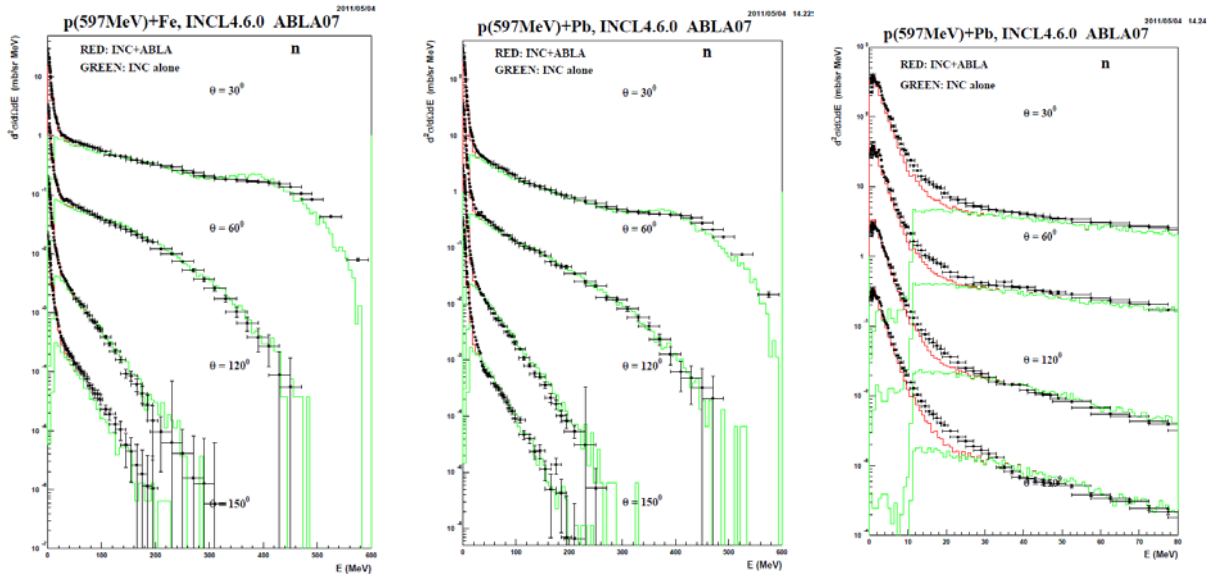

Figure 3: *Neutron double-differential cross-sections at different angles for p (597 MeV) + Fe (left) and Pb (center: full spectra, right: low energy part) from [Ami93] compared to the INCL4.5-ABLA07 model. The green curve is the contribution from INCL while the red one is the total one.*
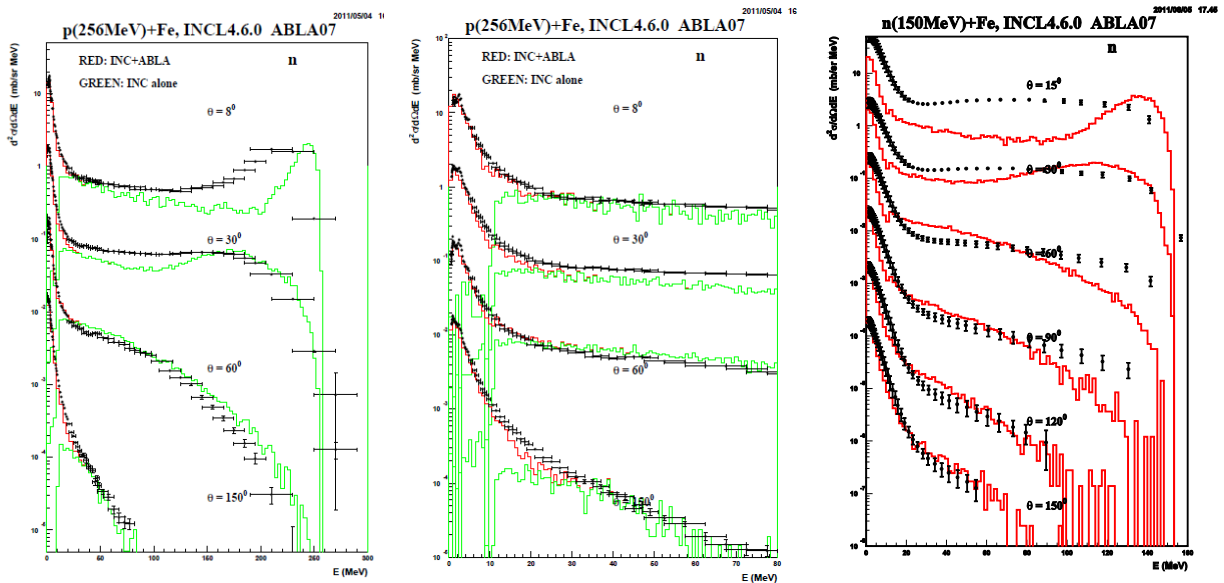

Figure 4: *Same as Fig. 3 but for p (256 MeV) + Fe (left: full spectra, center: low energy part) from [Mei93] and n (150 MeV) + Fe from [Ara07] (right).*

It can be concluded that, globally, the INCL4.5-ABLA07 model reproduces very well neutron production DDXS in the 150-600 MeV energy range and is certainly one of the best model implemented into high-energy transport codes. A few specific deficiencies do exist but generally does not affect the total production of neutrons, which is the important quantity for applications. The quality of the agreement with experimental data is however somewhat degrading with decreasing energy. An effort should be devoted to curing the spurious hole which appears around 10 MeV in the neutron spectra and becomes really visible at low incident energies, without degrading other observables. The reason for the deficiency concerning the forward angles and in particular the quasi

4

elastic peak should also be investigated, although this represents only a marginal part of the total neutron production cross-section.

3. Light charged particle emission

3.1 Protons

In the benchmark, the only data concerning proton production were n+Bi at 542 MeV [Fra90] and p+Ni at 175 MeV [Bud09]. Some other sets are however available in the domain we are interested in ANDES. Data at 392 and 300 MeV from [Kin05] are shown in Figs. 5 and 6 for Nb and C, respectively. The situation is rather similar to what was observed for neutron production. The agreement between the model and the experiment is rather good, slightly better at 392 than at 300 MeV, better for the niobium target than for carbon. The quasi elastic peak at forward angles is too sharp, as for neutron DDXS and seems to extend up to 55°. Data from [Bec76] at 558 MeV on different targets (not shown here) confirm the tendency that the model is less reliable for very light targets.
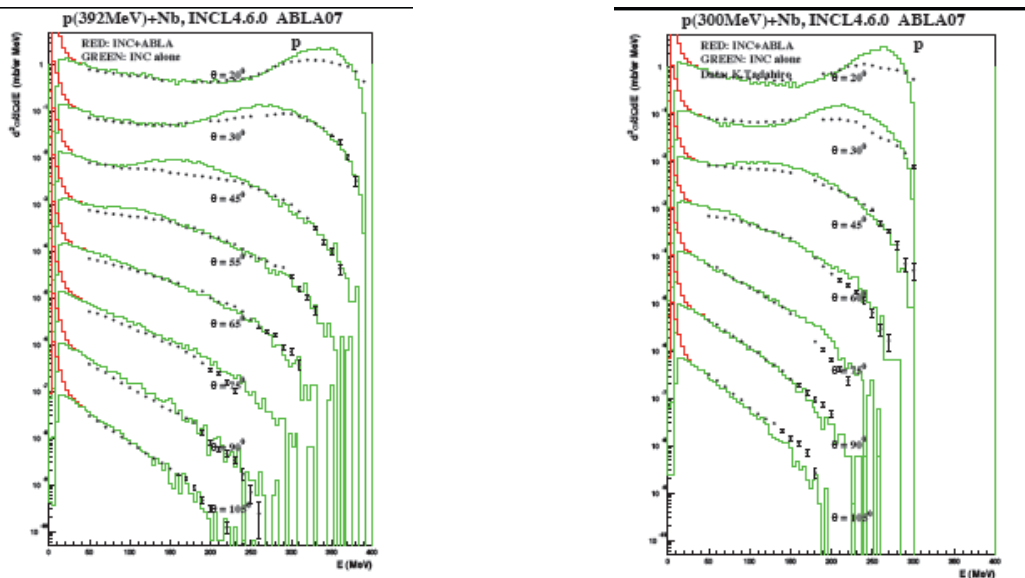

Figure 5*: Proton double-differential cross-section for p + Nb at 392 (left) and 300 MeV (right) from [Kin05] compared to INCL4.5-ABLA07.*

As regards lower incident energies, new data on neutron-induced reactions on Fe and Bi at 175 MeV have been obtained very recently at Uppsala by Bevilacqua et al. [Bev10] in the framework of ANDES. Proton and composite particle DDXS have been measured. The proton data are shown in Fig.7 together with data at the same energy obtained in proton-induced reactions. In the case of the neutron-induced DDXS, the raw experimental data are compared to a simulation with INCL4-ABLA07 implemented into MCNPX in order to take into account the actual energy spectrum of the neutron beam and the thickness of the targets. The effect of these experimental conditions will be discussed in section 3.3. Here again, it can be seen that the model globally agrees with the experiment, except at forward angles, as in the neutron DDXS case.
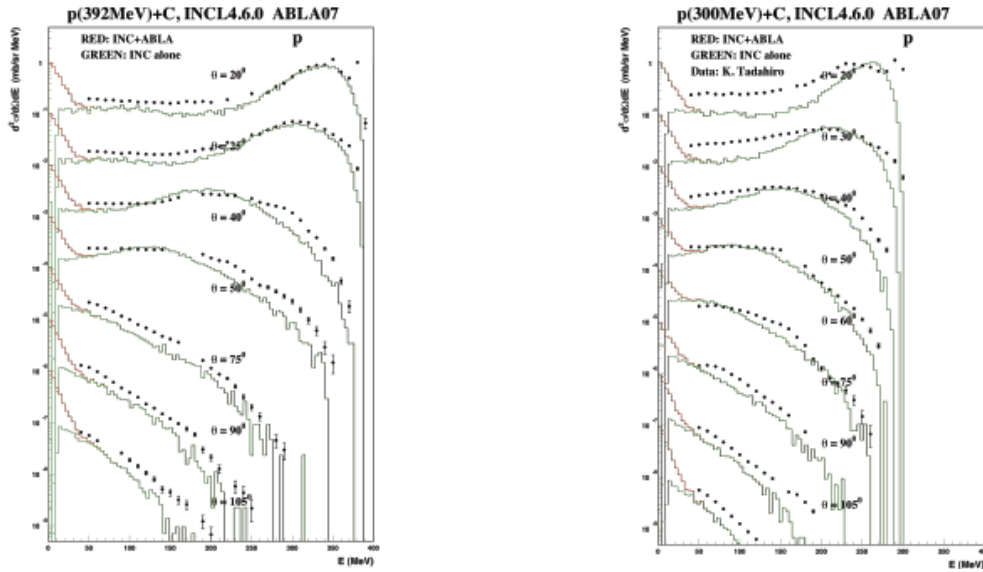
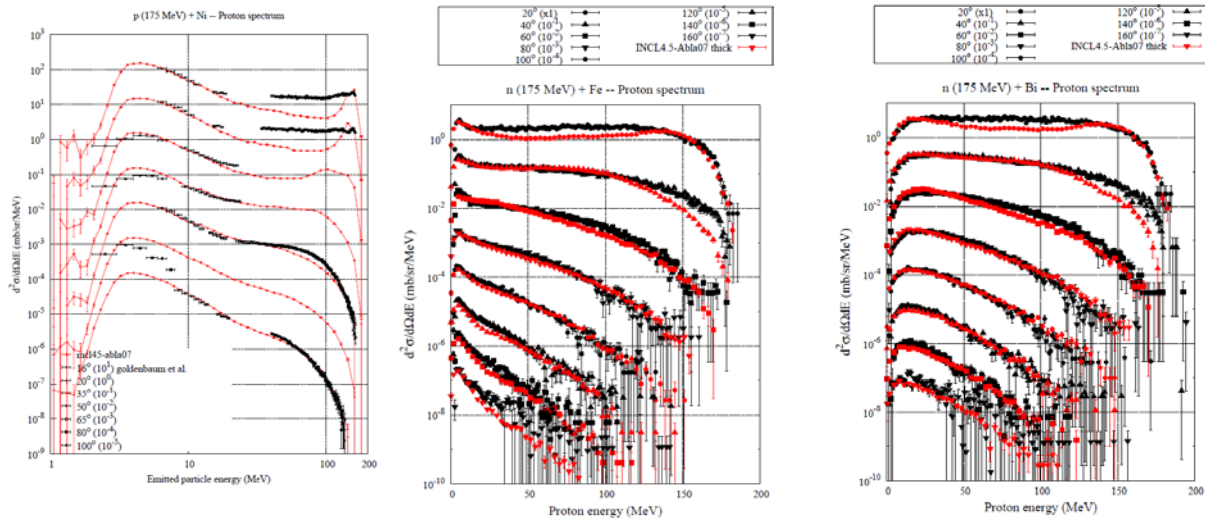**Figure 6**: *Same as Fig.5 but for p + C at 392 (left) and 300 MeV (right).*

Figure 7: *Proton DDXS in p (175 MeV) + Ni (left) from [Bud09], n (175 MeV) + Fe (center) and + Bi (right) from [Fra90] compared to INCL4.5-ABLA07 predictions. The calculated neutron-induced cross-sections are obtained with INCL4.5-ABLA07 implemented into MCNPX to take into account the neutron-energy spectrum and the target thickness.*

Globally, it can be said that proton production DDXS are predicted with more or less the same, actually rather good, accuracy and with the same specific deficiencies than neutron DDXS by INCL4.5-ABLA07. The benchmark showed more generally that, although the agreement with proton production cross-sections could be slightly less good than for neutron data, most of the models reproduce rather correctly the gross features of proton DDXS.

3.1 Light composite particles

- Lessons from the benchmark

The situation is rather different for light composite particle (d, t, ^{3}He and ^{4}He) production. In the benchmark, large differences between the predictions of the participating models were noticed. In particular, only a few models are able to predict correctly the high-energy tail observed in the experiments. Fig.8 shows examples taken from the few data sets in the energy of ANDES interest: alpha production DDXS in p+Ni at 175 MeV [Bud09] and p+Au at 160 MeV [Seg82]. Models like

6

INCL4.5 or CEM03 in which composite particles are formed through a coalescence mechanism in the intranuclear cascade stage are able to account for the high-energy tail while others, for instance the Bertini or Isabel models, are not.
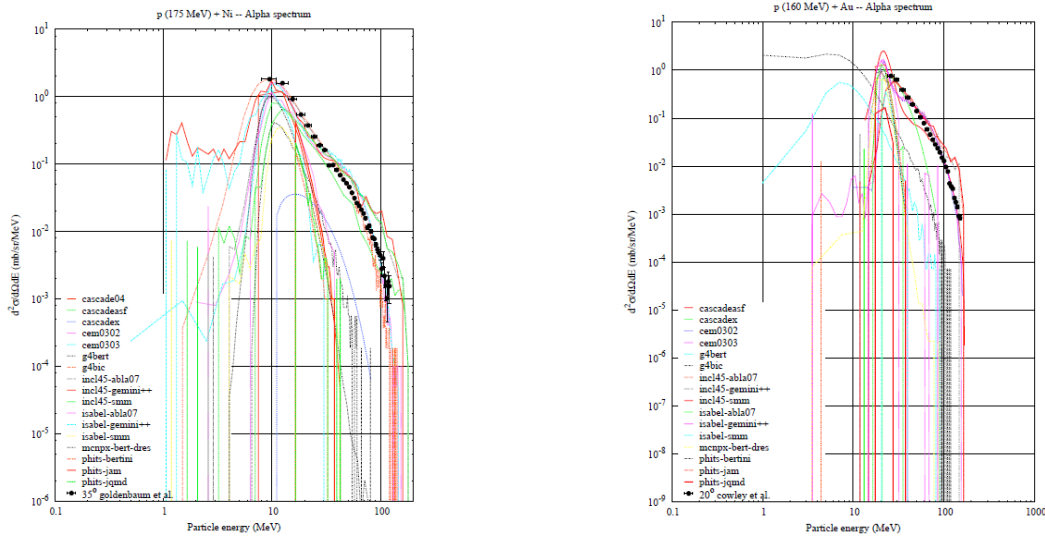

Figure 8: *Alpha double-differential cross-section for p (175 MeV) + Ni at 35° from [Bud09] (left) and p (160 MeV) + Au at 20° from [Seg82] (right) compared to all the models which participated to the IAEA benchmark.*

In the benchmark, separate ratings (from 0 to 4 points when going from very bad to very good agreement) were given for the different sets of data and for each type of light charged particles (including protons). The cases of p (175 MeV) + Ni and n (542 MeV) + Bi are displayed in Fig. 9. Models having no mechanism to produce high-energy composite particles have not been rated for these types. It can be seen that the predictions for the composite particle production is generally much less reliable than for protons. Often, a model was found to agree rather well with some sets of data and disagree with some other sets, making it difficult to draw conclusions on the best model. In a lot of cases, CEM03 [Mas05] gives better predictions than INCL4.5-ABLA07.
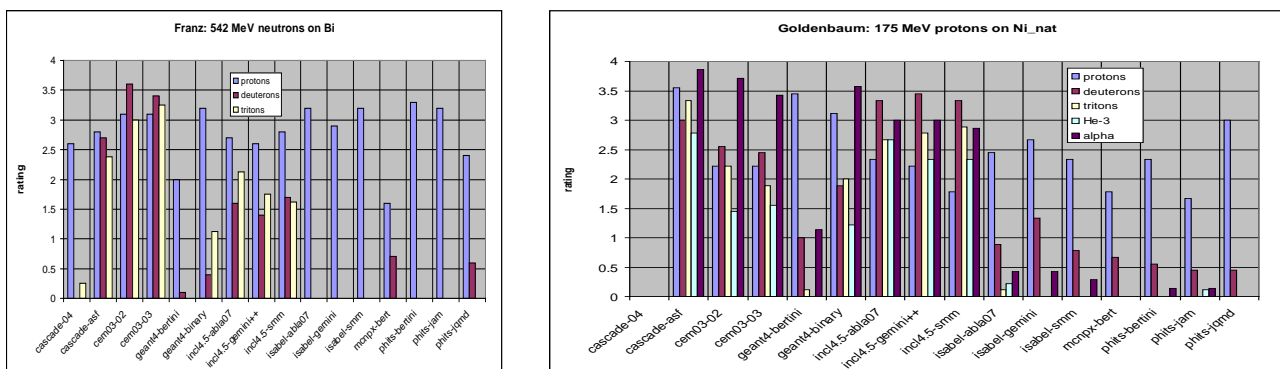

Figure 9: *Rating obtained for each model for the different types of light charged particles in the case of n (542 MeV) + Bi (left) and p (175 MeV) + Ni (right). Models having no mechanism to produce high-energy composite particles have not been rated for these types of LCPs.*

- Additional sets of data

In the energy range of our present interest, additional sets of data are sparsely available. In Fig.10, our model is compared to some of them. The shape of the deuteron DDXS in p (558 MeV) + Fe is

7

rather well reproduced at forward angles but not at large angles. The beginning of a rise below 100 MeV in the experimental data seems not realistic since the evaporation peak is not expected to extend to this energy value. For reactions induced by 200 MeV protons, the ^{3}He and ^{4}He DDXS measured on the Al target are predominantly in the evaporation region of the energy spectra and are rather well reproduced by the model. The Al experimental results are however a little suspicious at some angles since the evaporation component is expected to be isotropic. In the case of ^{4}He in p (200 MeV) + Au, according to our model, the measured spectra contain an important part originating from the INC stage which seems a little overestimated at backward angles.
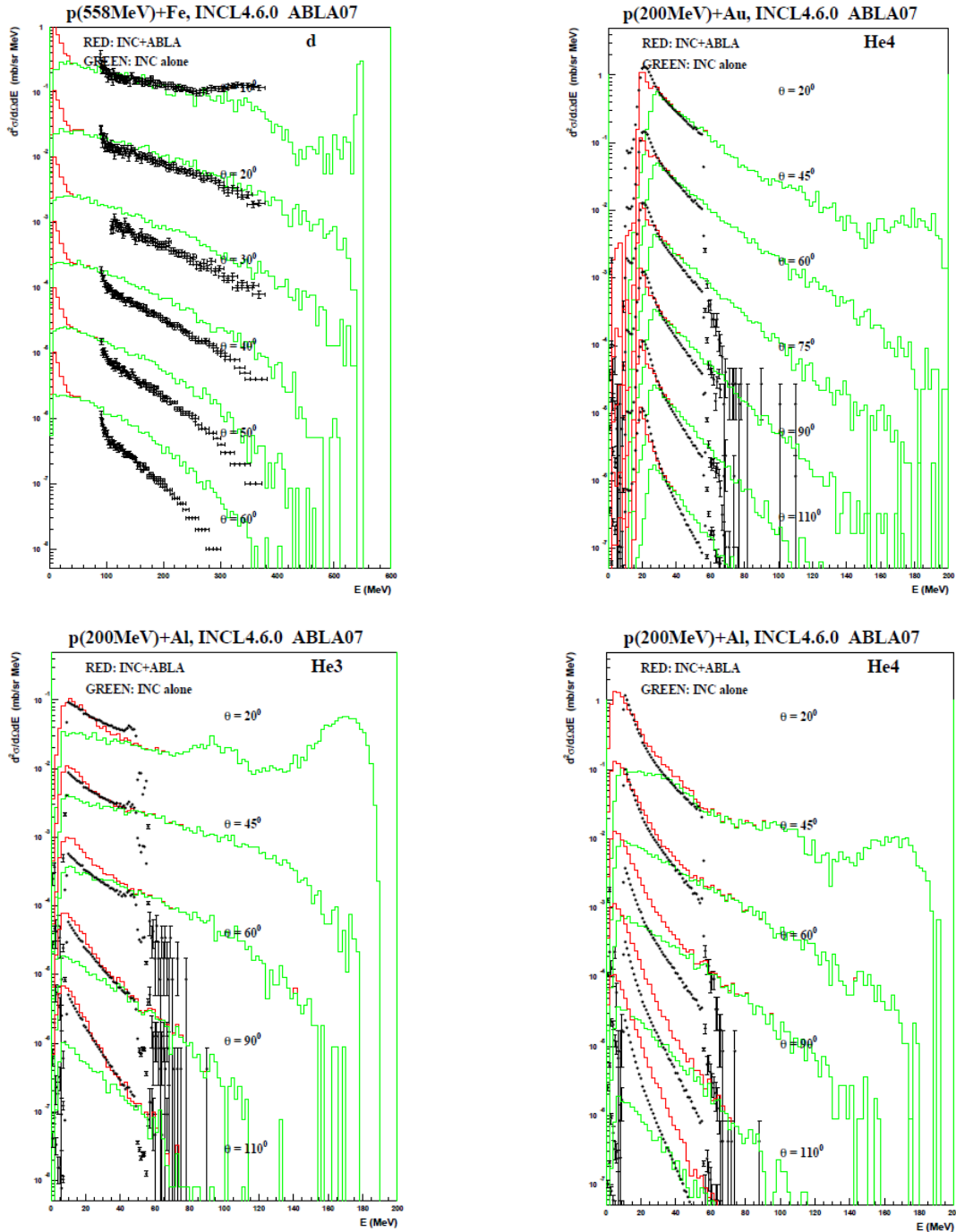

Figure 10: *Proton DDXS in p (175 MeV) + Ni (left) from [Bud09], n (175 MeV) + Fe (center) and + Bi (right) from [Bev10] compared to INCL4.5-ABLA07 predictions.*
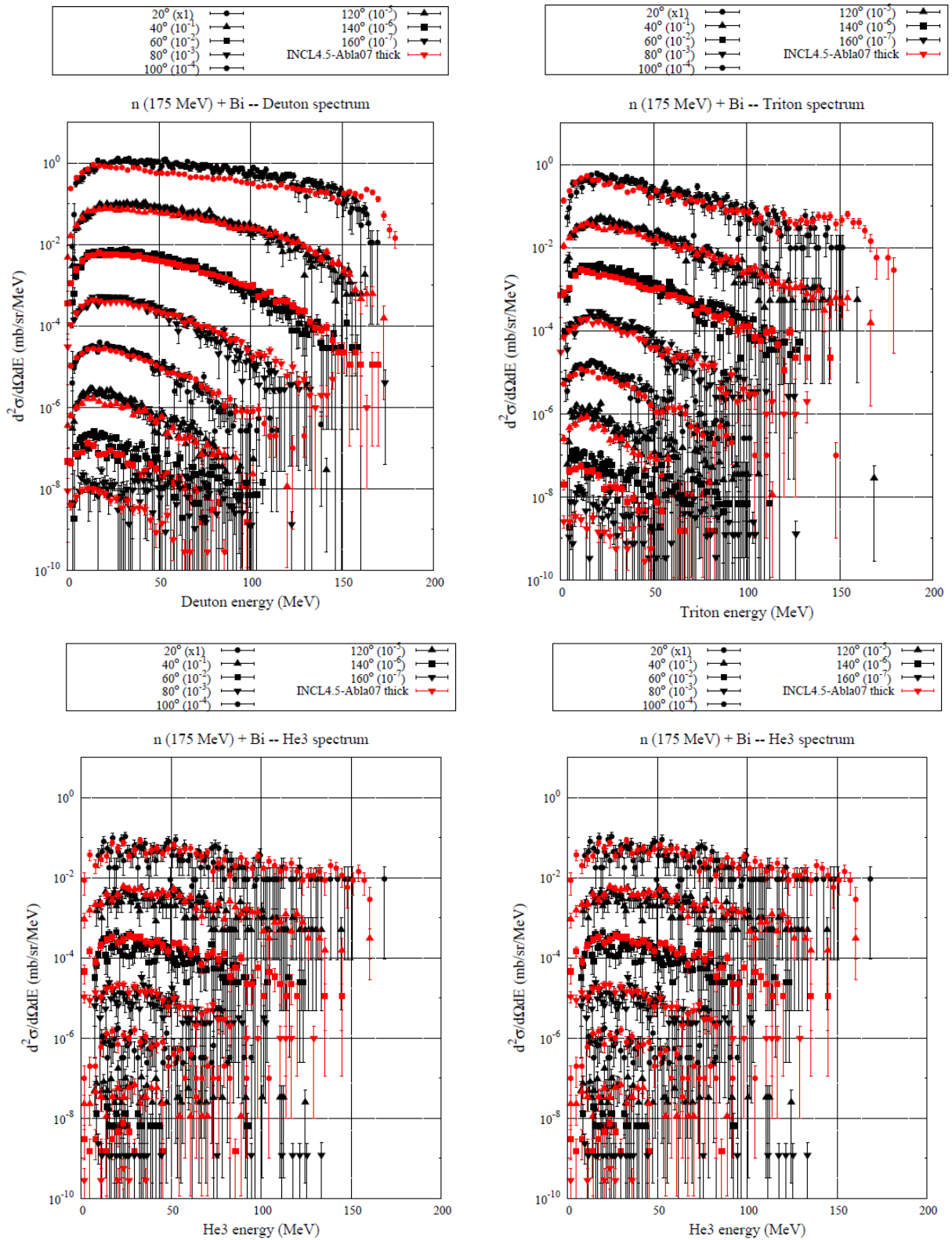
Figure 11: Composite particle production DDXS in n (175 MeV) + Bi from [Bev10] compared to INCL4.5-ABLA07 predictions. The calculated neutron-induced cross-sections (red points) are obtained with INCL4.5-ABLA07 implemented into MCNPX to take into account the neutron-energy spectrum and the target thickness. For the sake of clarity, error bars of 100% have been replaced by 99%.
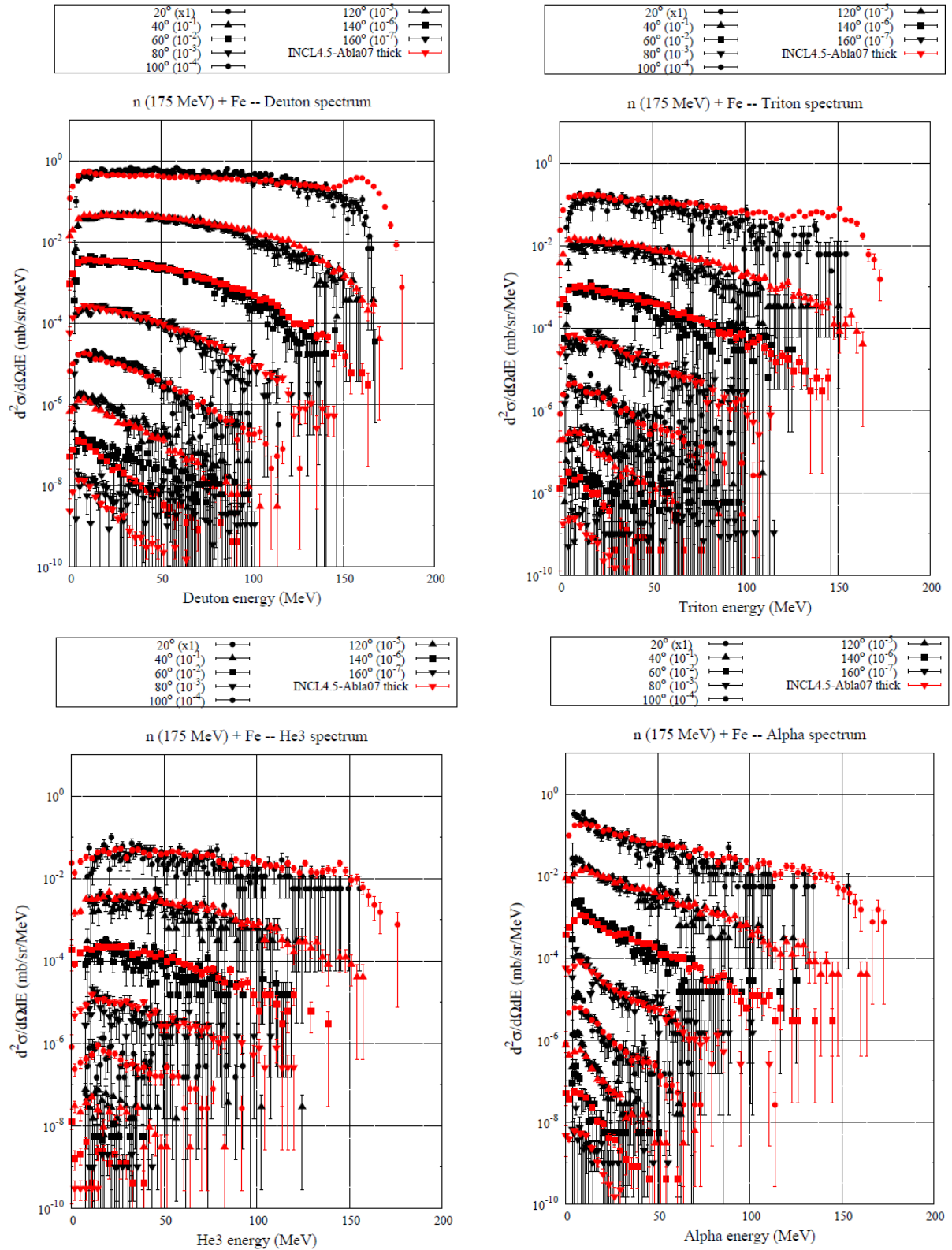
9

Figure 12: *Same as Fig.11 but for n (175 MeV) + Fe.*

More complete are the data from Bevilacqua et al. in which all the types of LCPs have been measured at 175 MeV in neutron-induced reactions on Fe an Bi targets. Our model (implemented into MCNPX) is compared to all the composite particle production DDXS obtained in this experiment in Figs. 11 and 12. It can be observed that the agreement is surprisingly good, with the exceptions of the very forward angles which exhibit a peak at high energy not seen in the data and sometimes at the largest

angles. The forward angle discrepancy could be related to the fact that, in our coalescence mechanism, the incident nucleon can pick-up other nucleons to form a cluster even if it did not interact through a nucleon-nucleon collision inside the nucleus, for instance in a very peripheral reaction. It should be noted that for composite particles taking into account the effect of the target thickness, and to a lesser extent the actual neutron spectrum, is even more important than for protons, as discussed in section 3.3.

- Total production cross-sections

Our model has been shown in the preceding section to reproduce rather well the composite particle production DDXS in the 150-600 MeV range, with some deficiencies generally at forward angles. It is also interesting to look at the total yields since this is important for the prediction of gas production in spallation targets, which is a concern either for material damage, in the case of helium, or for radioactivity release assessment, in the case of tritium. In [Ler10a], our model was compared to tritium and helium experimental excitation functions, in a wider energy range, together with predictions of CEM03 [Mas05] and Bertini-Dresner [Ber63]. The results are shown in Figs. 13 and 14 for, respectively, tritium and helium on iron and lead.
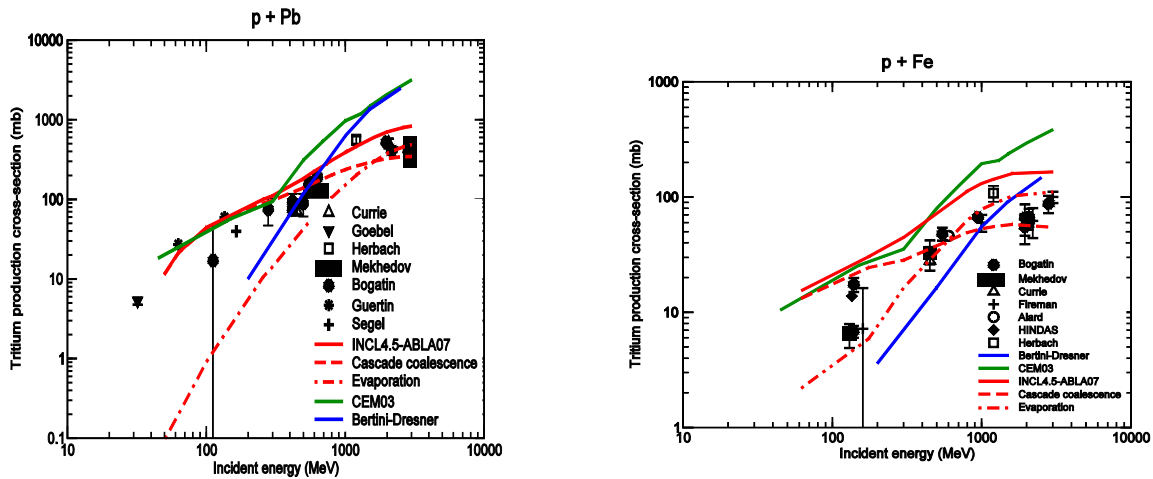

Figure 13: *Tritium production cross-section in lead (left) and iron (right). Calculations with the INCL4.5-ABLA07 (red line), Bertini-Dresner (blue line) and of the CEM03 (green line) models. The dashed and dot-and-dashed lines give the contributions of the cascade and evaporation, respectively, in INCL4.5-ABLA07. From [Ler10a].*

As pointed out in [Ler10a], predictions of helium and hydrogen production yields are globally much better than those from Bertini-Dresner, which is the default option of MCNPX, and than those of CEM03 in the case of tritium. It should be noted that the production of tritium (and also of ^{3}He) is dominated by the emission through the coalescence mechanism during the cascade stage, especially below 600 MeV, confirming the importance of taking it into account. However, there are large deviations between the different available experimental data sets on tritium, making it difficult to be sure of the conclusion. Clearly, new measurments of tritium production excitation functions would be very useful to establish the degree of reliability of the models.
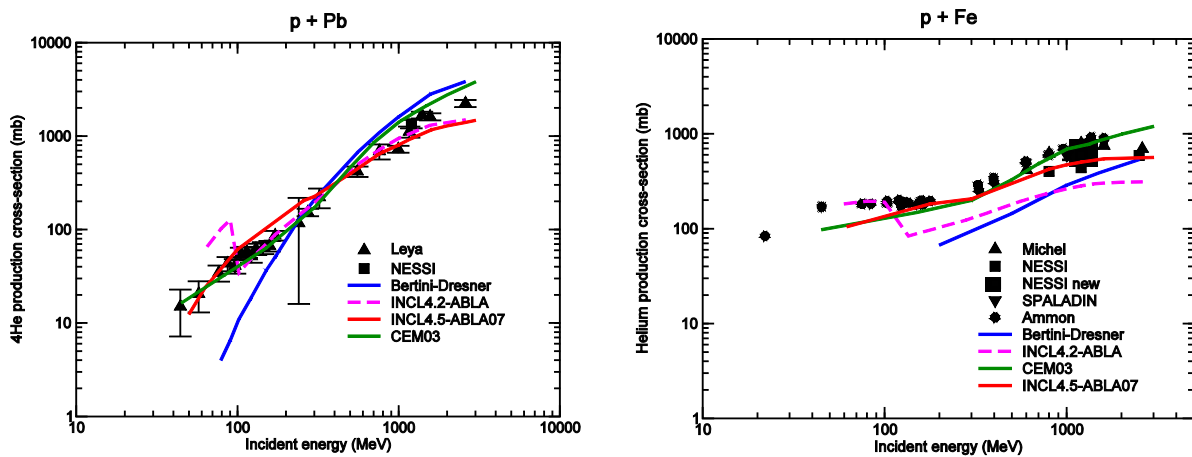
11

Figure 13*: Same as Fig.11 but for* ^{4}*He production cross-section in lead (left) and total helium in iron (right).*

3.3 Some comments on Bevilacqua's data

The experimental data from Bevilacqua et al. [Bev10] were obtained using a non-monoenergetic neutron beam on natural iron and bismuth targets. The thickness of the target was 0.375 and 0.5 mm, respectively. Actually, the incident neutron spectrum is composed of a broad peak around 175 MeV accompanied by a low energy tail containing as many neutrons as the 175-MeV peak. Therefore the raw data cannot be considered has "real" thin target data at 175 MeV. In [Bev10], the authors have tried to correct from both the thickness of the targets and the effect of the non-monoenergetic spectrum in order to obtain thin target data at 175 MeV. A first comparison of this corrected data did not agree at all with our model exhibiting discrepancies far larger than what could be expected, especially for the Bi target. Therefore, we decided to rather compare the raw experimental data to a simulation using MCNPX (in which our model is implemented) in order to account for this effects. This is what has been shown in Figs. 7, 11 and 12.

In Figs. 15 and 16, we show a comparison between the raw and the corrected experimental data together with the full simulation and the "real" thin target DDXS at 175 MeV. In principle, if the correction of the raw data to obtain thin target data at 175 MeV is well under control, we would expect the ratio between the thin-target 175 MeV data and the corrected thick-target data with the complete spectrum to be similar in the experiment and in the simulation. This is also equivalent to say that the corrected data should compare with the thin target calculation the same way the raw data compares to the full simulation, i.e. blue and green points should compare as black and red points do. This is more or less true for protons but some large discrepancies, especially in the case of helium production in bismuth, between the thin target calculation and the corrected DDXS are found for composite particles suggesting that something may be not properly taken into account in the correction. The effect of the incident not mono-energetic energy spectrum is visible in the smearing out of the high-energy peak at forward angles.
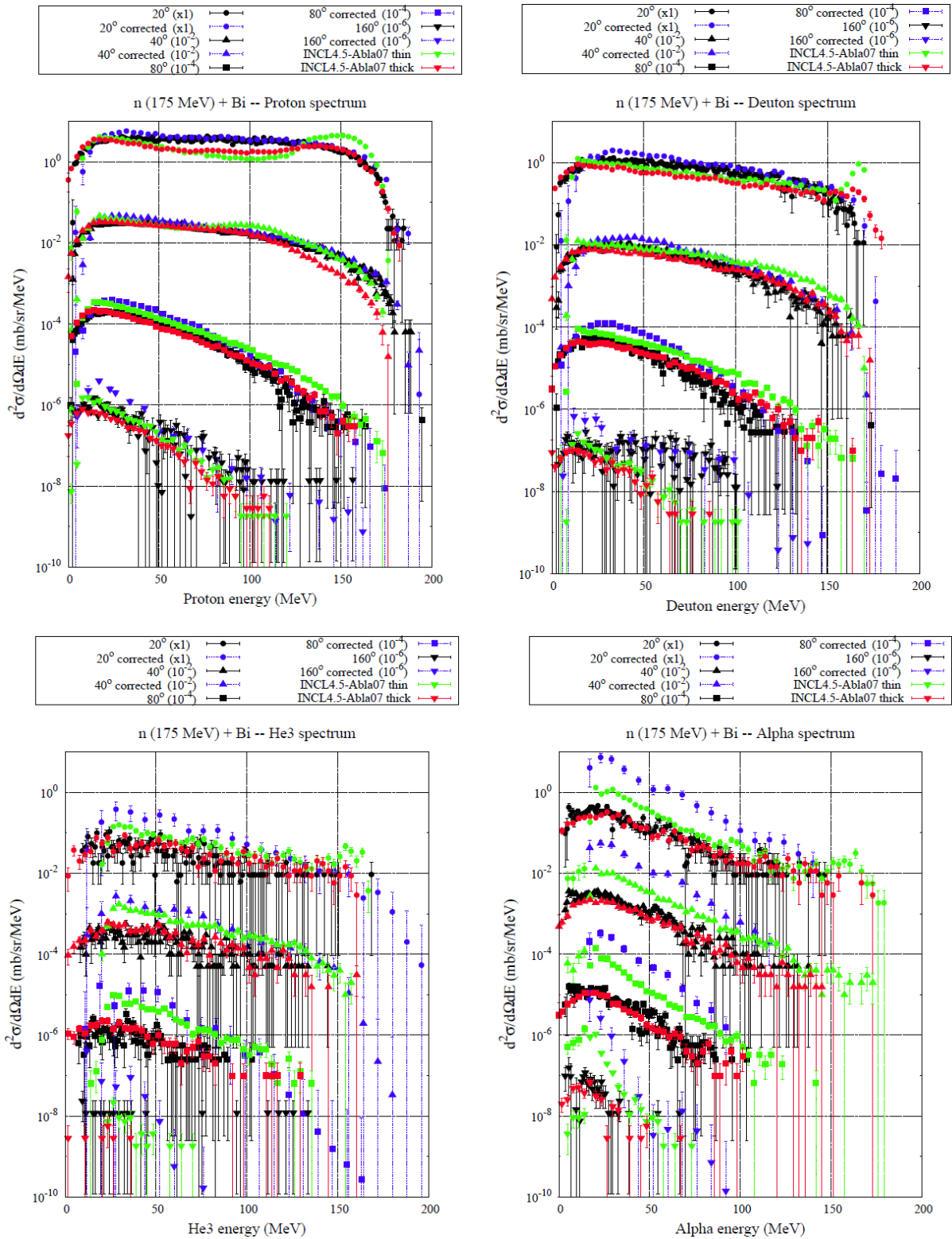
Figure 15: *Proton, deuteron, ³He and ⁴He DDXS in n (175 MeV) + Bi from [Bev10] compared to INCL4.5-ABLA07 predictions. Black dots are the raw measured data. Blue dots are the DDXS corrected by the authors. The green points are "real" thin target DDXS at 175 MeV calculated with our model, while red ones are obtained with INCL4.5-ABLA07 implemented into MCNPX to take into account the neutron-energy spectrum and the target thickness.*
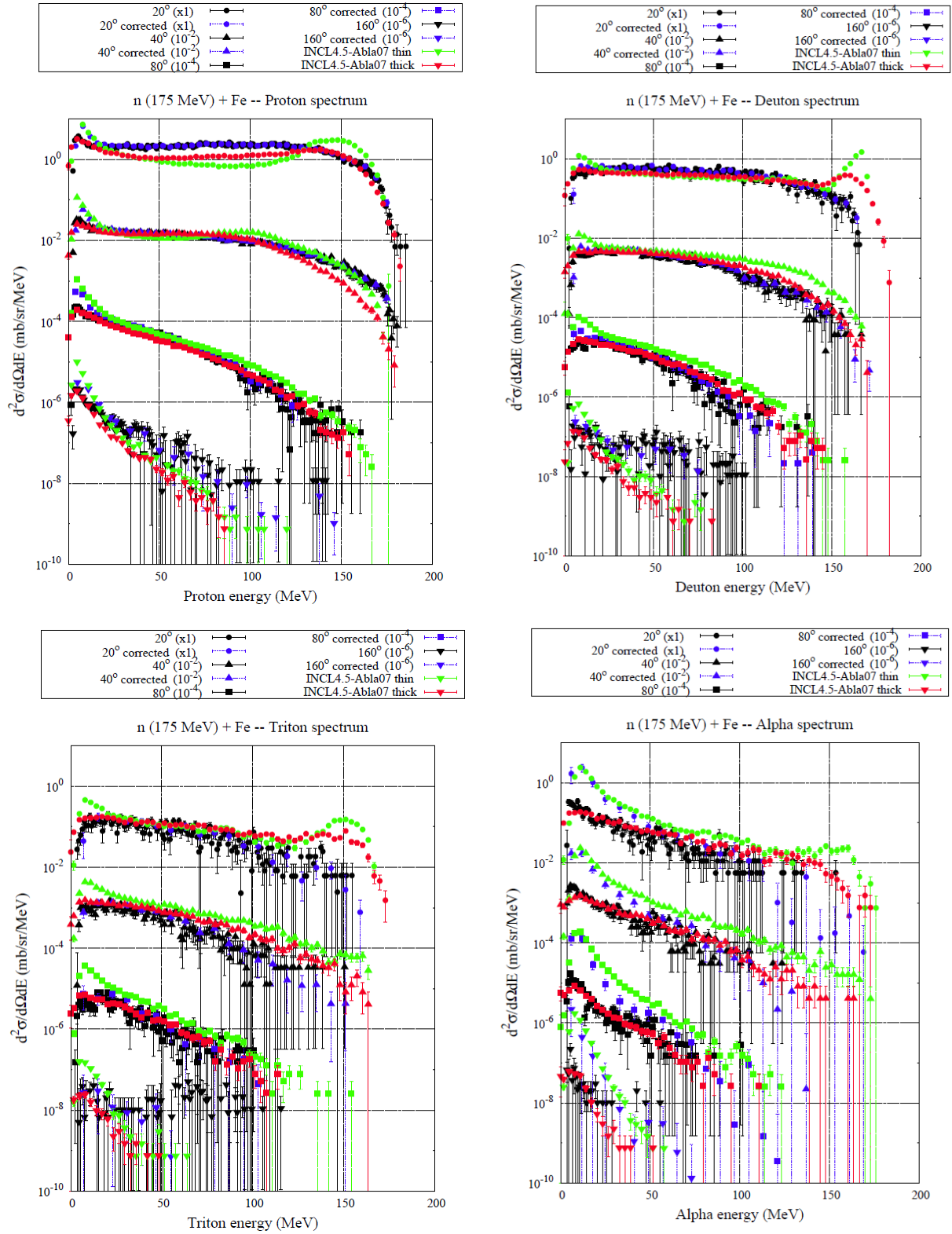
13

Figure 16*: Same as Fig. 11 but for proton, deuteron, triton and ^{4}He DDXS in n (175 MeV) + Fe.*

4. Intermediate mass fragment DDXS

The emission of composite particles heavier than alphas, also called intermediate mass fragments (IMFs) and often defined as elements with charge between 3 and 10, is observed in reactions with incident energies between 150 and 600 MeV. Among them are radioactive isotopes as ^{7}Be and ^{10}Be

that contribute to the radiotoxicity of spallation targets in the short and long terms. IMFs mainly originate from the de-excitation stage and can be described through a generalized evaporation model or by an asymmetric fission mechanism. However, the lightest of them exhibit an energy spectrum extending to rather high values not explainable by these mechanisms. This is why the coalescence mechanism of INCL4.5 has been extended to clusters with masses up to 8 in the last version [Cug09].
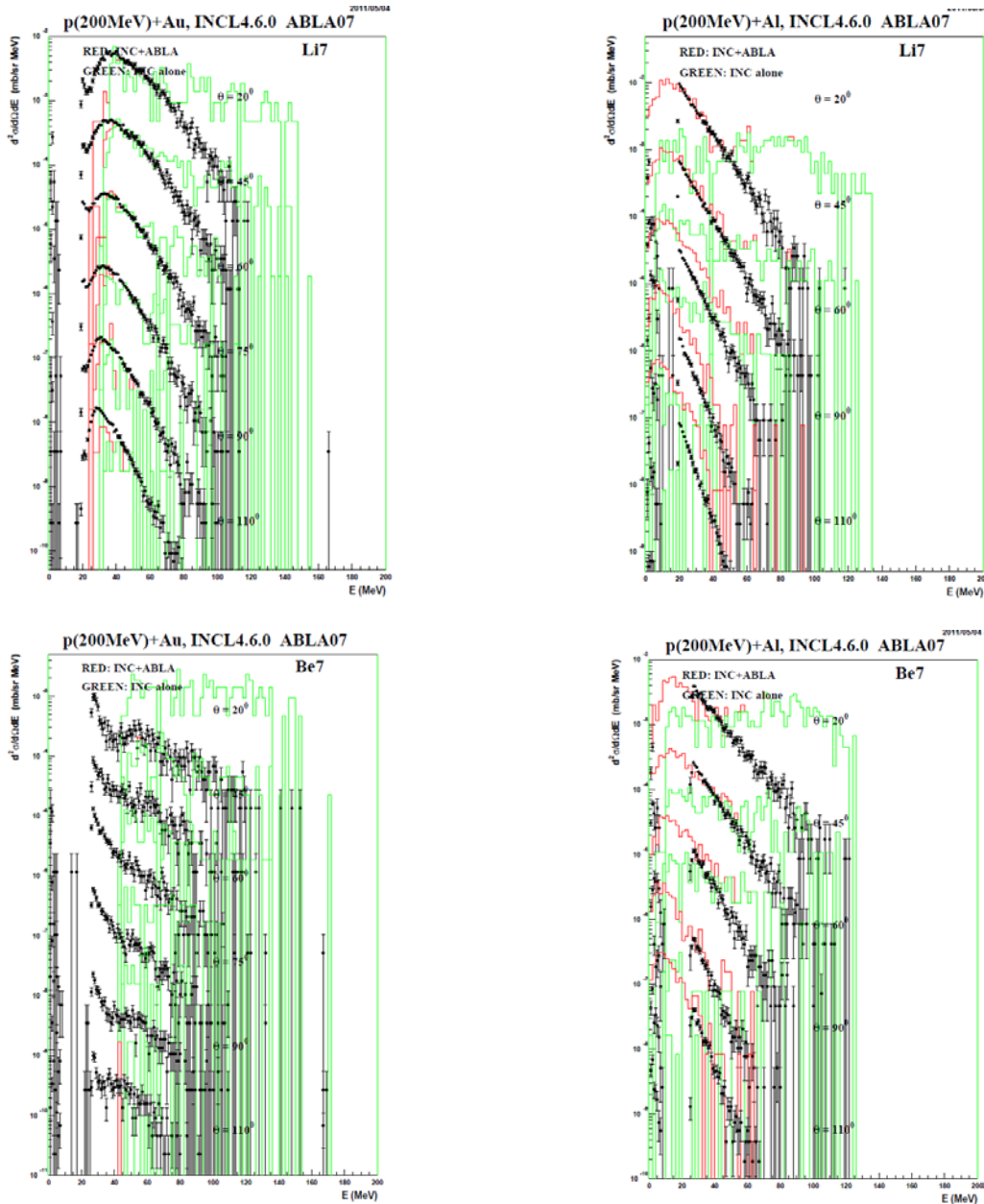

Figure 17: *^{7}Li and ^{7}Be DDXS in p (200 MeV) + Al (right) and Au (left) from [Mac] compared to INCL4.5-ABLA07 predictions.*

There was no data on IMF DDXS proposed for comparison to the models in the IAEA benchmark. Actually, only a few of the available models, among which ABLA07, have mechanisms to produce IMFs during the de-excitation and, to our knowledge, INCL4.5 is the only one having the capability to emit high-energy IMFs. Actually, the coalescence model was adjusted to reproduce reasonably well data at high incident energies [Cug10]. In Fig.17, we compare the predictions of INCL4.5-ABLA07 to experimental data obtained at 200 MeV [Mac06] on Au and Al targets. Clearly, our coalescence mechanism seems to be much too strong and maybe not necessary in these data. On the contrary,

15

the low energy part of the spectra is rather well reproduced by the component coming from ABLA07, in the case of Al but not for the Au target, for which there is nearly no emission from the de-excitation stage.

5. Residues

5.1 Residue distributions

The experiments performed at the Fragment Separator (FRS) at GSI, during the FP5 HINDAS and FP6-NUDATRA projects, using the reverse kinematics technique, allowed measuring complete isotopic distributions. In the IAEA benchmark, these data were compared to all the participating models. The performance of the different models were evaluated through a coarse eye-guided rating, distinguishing different product nuclide regimes: target-near products, spallation products with masses exceeding half the target mass, light products with masses (much) smaller than half the target mass, fission products (for lead and uranium), light nuclei (A < 10). Separate ratings were done for mass and charge distributions, on the one hand, and for isotopic distributions, on the other hand. They are shown in Fig.18. Clearly, the situation is poorer than for neutron and charged particle cross-section and only few of the models, among which INCL4.5-ABLA07, have a positive rating. It is interesting to notice that calculations done with the same INC code coupled to different de-excitation models can obtain very different rates, showing the high sensitivity of residue production to the de-excitation stage.
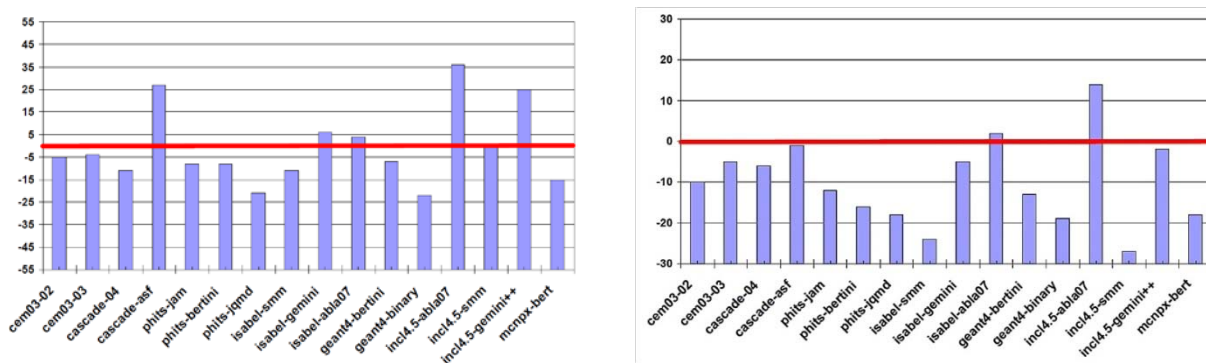

Figure 18: Rating of the results for predicting the mass and charge distributions (left panel), the isotope distributions (rightpanel) measured by inverse kinematics for iron, lead, and uranium. From [Dav10a, Ler10b].

In the 150-600 MeV domain, only three systems were studied at FRS: Fe (300 and 500 MeV/u) [Vil07] and Pb (500 MeV/u) + p [Aud06]. In the left and central panels of Fig.19, taken from the IAEA benchmark, the mass distributions for two of these systems are compared to all the models, confirming the large discrepancies between the different models, which increase when going towards lower residue masses. In the right panel, the prediction of our model is plotted together with the experimental results for Fe (500 MeV/u) + p. A very good agreement is observed. Isotopic distributions for the heaviest elements in Fe and Pb (500 MeV/u) + p are presented in Fig.20 accompanied by calculations with INCL4.5-ABLA07. Here again, we can see the quality of the agreement between the model and the experimental data. However, a careful look at the isotopic distributions of the elements close to Pb shows significant discrepancies, which can be problematic since these residues represent the largest part of the total cross section and are generally the main contributors to the activity of an ADS spallation target [Dav10b]. In fact, at 500 MeV the situation is

somewhat better than at 1 GeV (not shown here), as it is confirmed by some comparisons with measured excitation functions (see below).
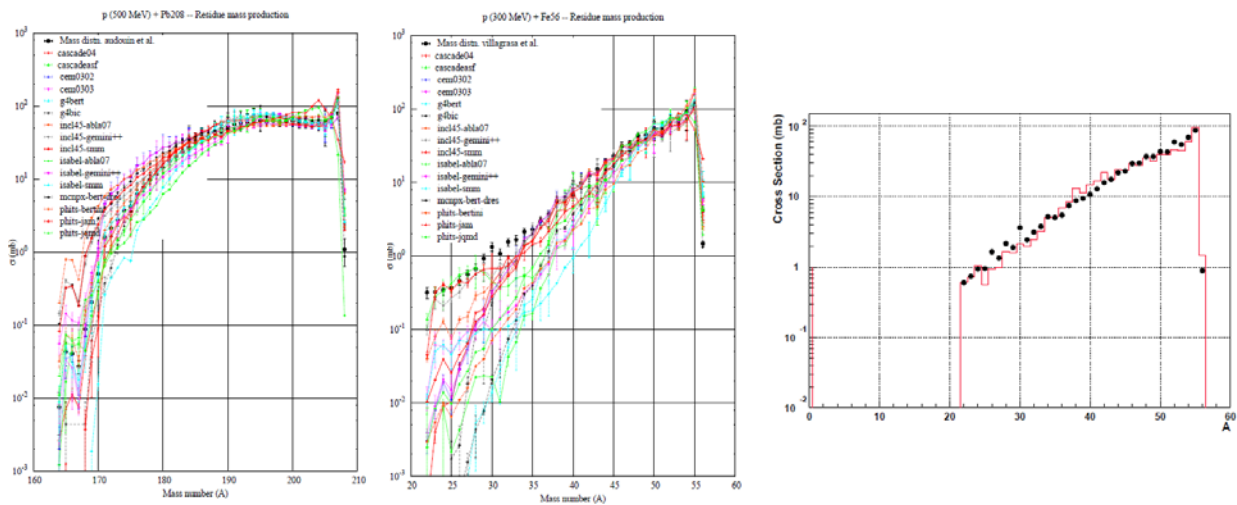

Figure 19: Mass distribution measured for the ^{208}Pb (500 MV/u)+p (left panel) [Aud06] and ^{56}Fe (300 MeV)+p [Vil07] (central panel) compared to all the models which participated to the IAEA benchmark and for ^{56}Fe (300 MeV)+p [Vil07] (right panel) compared to INCL4.5-ABLA07
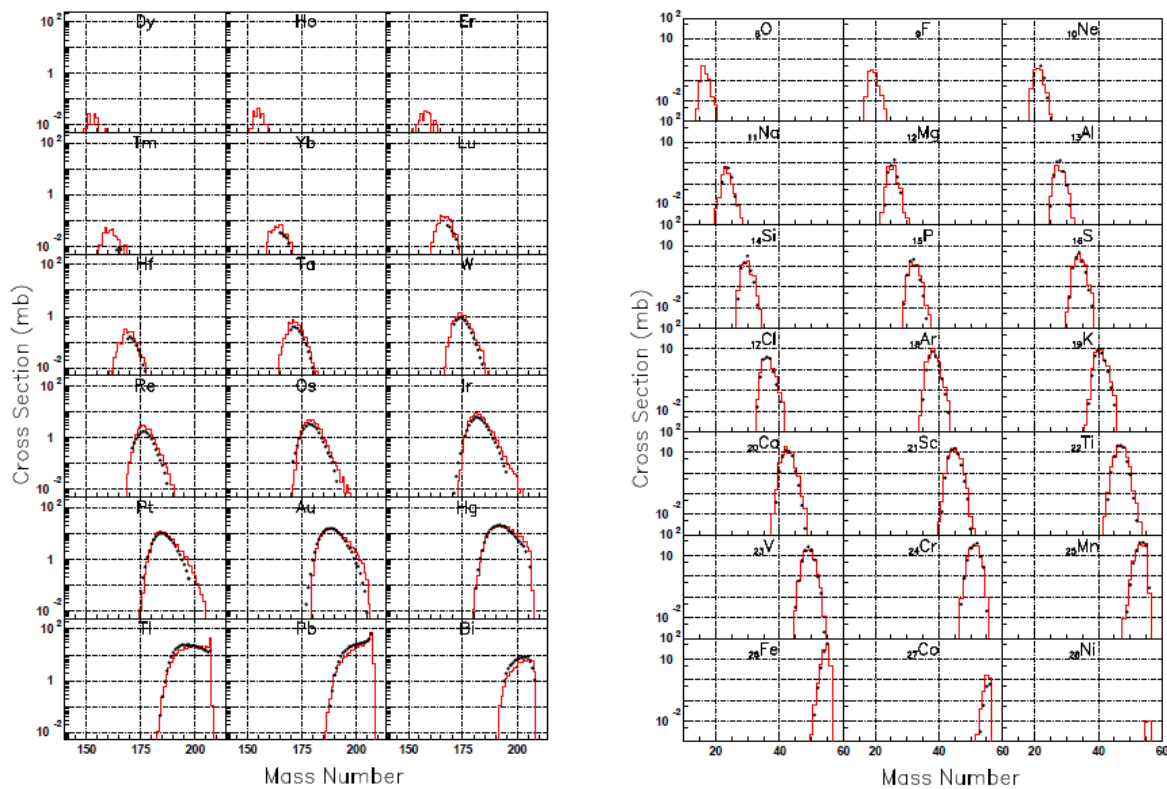

Figure 20: Isotopic distribution of the heaviest elements for the ^{208}Pb(500 MV/u)+p [Aud06] (left) and ^{56}Fe (500 MeV)+p [Vil07] (right) + compared to INCL4.5-ABLA07.

- Excitation functions

Excitation functions, i.e. production cross-sections of a given isotope as a function of incident energy, are especially useful to test the evolution of the model reliability with energy. They exist only for specific nuclei and are often cumulative yields along a decay chain but they are often representative of isotopes of particular concern for radioactivity assessment. A large number of excitation functions have been compared to the models in the IAEA benchmark. Examples are given in Fig.21, illustrating

some general trends i.e. that the deviation between the models and the experimental data can be very large and that the conclusions on the quality of a given model may vary from one isotope to another. Generally, the discrepancies are considerably larger for fission fragments than for heavy residues. Some models are rather good in a given incident energy range but have not a correct dependence in the whole incident energy domain.
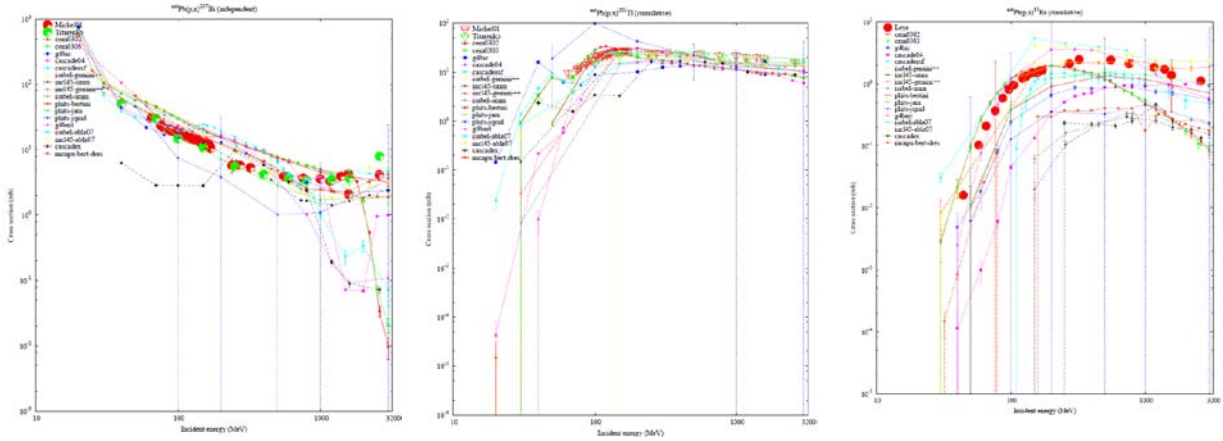

Figure 21: Excitation functions for the production of ^{207}Bi (left), ^{202}Tl (center) and ^{85}Kr from a Pb target bombarded by protons compared to all the models in the IAEA benchmark.
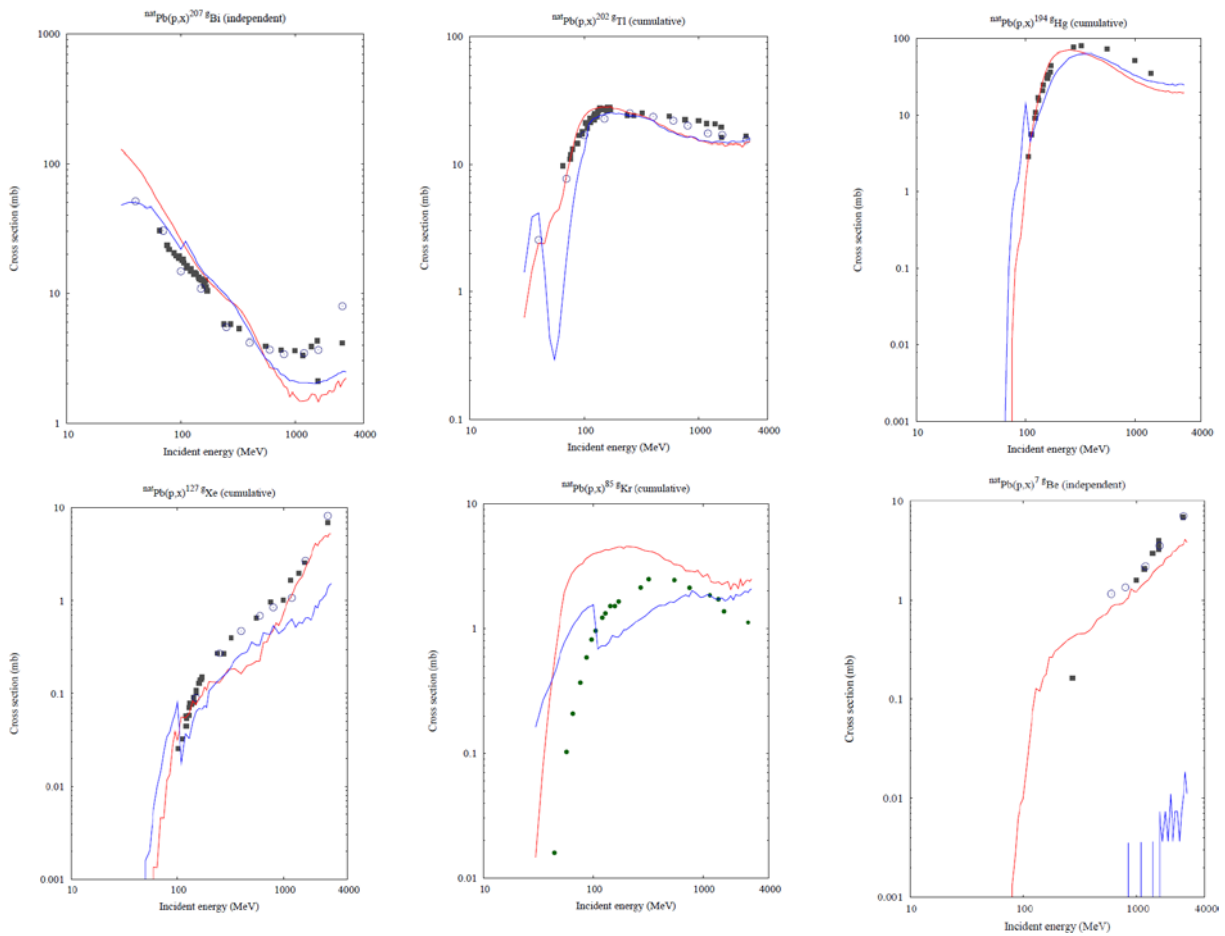

Figure 22: Measured excitation functions (points) for the production of, from left to right and top to bottom, ^{207}Bi, ^{202}Tl, ^{194}Hg, ^{127}Xe, ^{85}Kr and ^{7}Be from a natural Pb target bombarded by protons [Ley05, Tit06] compared to INCL4.5-ABLA07 (red curve) and the old version INCL4.2-ABLA (blue curve).

18

As regards the comparison of INCL4.5-ABLA07 to excitation functions, examples are shown on Figs. 22 and 23 for proton on lead and iron, respectively. Results from the old version of the code, INCL4.2-ABLA, are also displayed to highlight the improvements achieved during NUDATRA. Generally, the agreement with the data is not bad and stays within a factor smaller than 2 and the shape of the excitation function is well reproduced by our code, indicating that the energy dependence of the model is rather good. However, significant discrepancies are found for some isotopes, in different energy region depending on the considered nucleus. For lead, the model shows a tendency to underpredict the isotopes close to lead in our energy range of interest. This corroborates the conclusions drawn from the comparison to isotopic distributions. The largest discrepancies are found for some of the fission fragments and are often more important at low energies. The model agrees reasonably well with the ^{7}Be excitation function at high energies and overestimates the point around 200 MeV. This may be related with what was observed in Fig. 17 for the DDXS in p+Au.
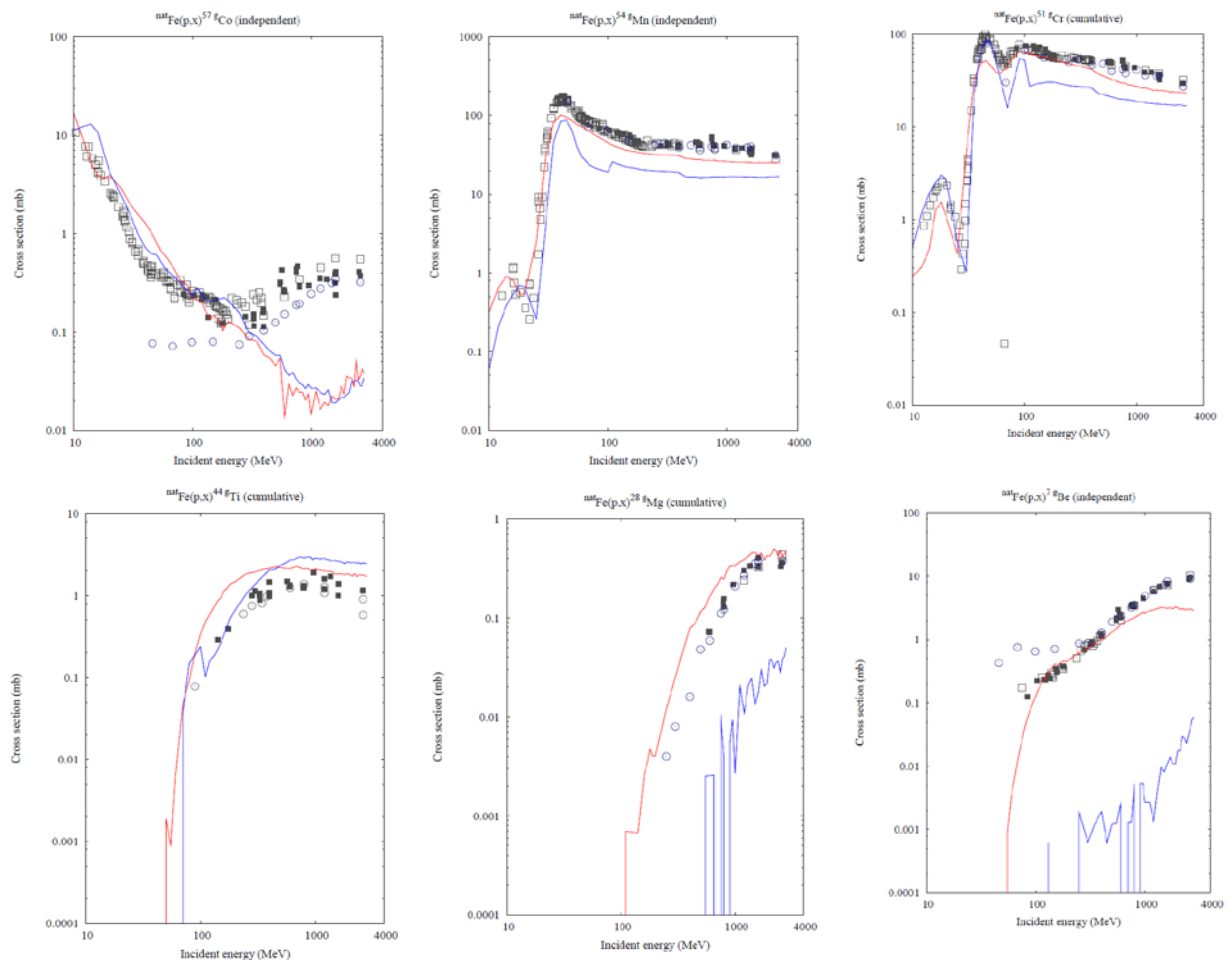

Figure 23: Measured excitation functions (points) for the production of, from left to right and top to bottom, ^{57}Co, ^{54}Mn, ^{51}Cr, ^{44}Ti, ^{28}Mg, and ^{7}Be from a natural Fe target bombarded by protons [Tit08, Mic02] compared to INCL4.5-ABLA07 (red curve) and the old version INCL4.2-ABLA (blue curve).

In the case of iron, the global agreement is even better than for lead. Specific discrepancies concern the prediction of cobalt isotopes above 200 MeV, an overprediction of some isotopes around masses 20 to 45 and an underprediction of intermediate mass fragments at high energies.

6. Conclusion

In this report, we have used the results from the recent IAEA benchmark and additional experimental data sets to evaluate the quality of the predictions of INCL4.5-ABLA07 combination of models in the 150-600 MeV range and, when possible, compared to other models. Globally, the predicting capability of our model is rather good and, generally, better than other models available in high-energy transport codes. However, a few specific deficiencies have been pointed out, which generally tend to increase as the incident energy decreases. They concern:

1) forward angle DDXS whatever the type of considered particle, and, in particular the prediction of quasi-elastic peaks
2) the appearance of a spurious hole around 10 MeV in neutron energy spectra, which becomes more and more important as the incident energy decreases
3) a less good agreement of the models for composite particle DDXS
4) a clear overestimation of the production of intermediate mass fragments through our coalescence mechanism
5) a significant underprediction of some residues close to the target nucleus
6) a difficulty to properly predict fission fragment all along the energy range

The goal of Task 4.4 will be to cure these deficiencies, as far as possible without degrading the good results obtained in other observables. It should be recalled that in our models, parameters are not adjusted for each different set of data, but fixed once for all based on physics considerations and comparison with the whole bulk of data.

The other point that should be addressed concerns composite particle-induced reactions. As discussed in section 3.1, composite particle DDXS exhibit a significant high-energy tail. In a thick target, these particles will undergo secondary reactions that could lead to the production of isotopes with two additional charge compared to the target nucleus. In the case of Pb-Bi, this means the production of polonium and astatine isotopes, which are a major concern for radioprotection. Up to now, although INCL4.5 is able to treat reactions with projectiles up to helium, it was not really tested and the first attempts to calculate these isotope productions did not give satisfying results. Some effort will be devoted in Task 4.4 to improve the treatment of composite particle reactions.

References

[Ami93] W.B. Amian et al., Nuclear Science and Engineering, Vol.115, p.1 (1993)

[Ara07] H. Arakawa et al., Conf.: Symp.on Nuclear Data, Tokai, Japan, Jan. 2007, p.V05 (2007) Japan

[Aud06] L. Audouin et al., Nucl. Phys. A768 (2006) 1

[Bec76] S.M. Beck and C.A. Powell, Report NASA-TN-D-8119, 1976

[Ber63] H.W. Bertini, Phys. Rev. 131, 1801 (1963); L. Dresner, ORNL Report ORNL-TM-196 (1962).

[Bev10] R. Bevilacqua et al., Radiation Measurements, Volume 45, Issue 10 (2010) 1145

[Bou02] A. Boudard et al., Intranuclear cascade model for a comprehensive description of spallation reaction data, Phys. Rev. C66 (2002) 44615.

[Bud09] A.Budzanowski et al., Phys. Rev. C80(2009)054604

[Cug09] J. Cugnon, A. Boudard, S. Leray, D. Mancusi, "Results obtained with INCL4", in: Proceedings of the International Topical Meeting on Nuclear Research Applications and Utilization of Accelerators, Vienna, May 4–8, 2009.

[Cug10] J. Cugnon et al., "Final report and code of an improved version of INCL4-ABLA", EUROTRANS deliverable D5.19, 2010.

[Dav10a] J.C. David et al, "A new benchmark of spallation models", Tenth meeting of the task force on Shielding Aspects of Accelerators, Targets and Irradiation Facilities, CERN, June 2-4, 2010

[Dav10b] J.C. David, S. Lemaire and S. Leray, "Activation calculations for the MEGAPIE target with INCL4 and ABLA, and comparison with other codes", EUROTRANS deliverable D5. 9 (2010)

[DeB11] De Bruyn D., Aït Abderrahim H., Baeten P., Fernandez R., "MYRRHA, the Multi-purpose Hybrid Research Reactor for High-tech Applications", In: ICAPP'11 "Performance & flexibility:the power of innovation", Nice, France, 2-6 May 2011, France, Omnipress, 2011, p. 472

[Enq01] T. Enqvist et al., Nucl. Phys. A686 (2001) 481

[Fra90] J. Franz et al., Nucl. Phys. A 510 (1990) 774

[Hen05] [7] J.S. Hendricks et al., "MCNPX extensions version 2.5.0", Los Alamos Report LA-UR-05-2675 (2005).

[IAE09] http://www-nds.iaea.org/spallations

[Jun98] A.R. Junghans *et al.*, Nucl. Phys. A629, 635 (1998).

[Kel09] A. Kelić, V. Ricciardi, K.-H. Schmidt, "Results obtained with ABLA007", in: Proceedings of the International Topical Meeting on Nuclear Research Applications and Utilization of Accelerators, Vienna, May 4–8, 2009.

[Kin05] T. Kin et al., Phys. Rev. C 72, 014606 (2005)

[Ler10a] S. Leray et al., "Improved modelling of helium and tritium production for spallation targets", Nuclear Instruments and Methods in Physics Research B 268 (2010) 581.

[Ler10b] S. Leray et al., "Results from the IAEA benchmark of spallation models", Int. Conf. on Nuclear Data for Science and Technology 2010 (ND2010) Jeju, Korea, 26-30 April 2010.

[Ley05] I. Leya et al., Nucl. Instr. and Meth. B 229 (2005) 1

[Mac06] H. Machner et al., Phys. Rev. C 73, 044606 (2006)

[Mas05] S.G. Mashnik et al., AIP Conf. Proceedings 768, 1188 (2005)

[Mei93] M. Meier et al., Nucl. Sci. Eng. 110 (1993) 289

[Meu05] J.-P. Meulders, A. Koning and S. Leray, HINDAS EU Contract FIKW-CT-00031, final report, January 2005, (http://www.theo.phys.ulg.ac.be/~cugnon/Final_Scientific_Report_HINDAS.pdf).

[Mic02] R. Michel et al., Nucl. Sci. Tech., Supplement 2 (2002) 242

[NUD04] EUROTRANS, EUROpean Research Programme for the TRANSmutation of High Level Nuclear Waste in an Accelerator Driven System, Contract no. FI6W-CT-2004-516520, DM5-NUDATRA.

[Seg82] R.E. Segel et al., Phys. Rev. C 26, 2424–2432 (1982)

[Sco90] W. Scobel et al. Phys. Rev. C 41, 2010–2020 (1990)

[Tit06] Y. E. Titarenko et al., Nucl. Instr. and Meth. A562 (2006) 801

[Tit08] Y. E. Titarenko et al., Phys. Rev. C 78 (2008) 034615

[Vil07] C. Villagrasa-Canton, et al., Phys. Rev. C 75 (2007) 044603